

Multispectral Imaging for Diagnosis & Treatment

Gary E. Carver*^a, Sarah A. Locknar^a, William A. Morrison^a, Daniel L. Farkas^{b,c}

^aOmega Optical, 21 Omega Drive, Brattleboro VT, USA 05301;

^bDept. of Biomedical Engineering, University of Southern California, Los Angeles CA, USA 90089

^cSpectral Molecular Imaging, 250 N. Robertson Blvd., Beverly Hills CA, USA 90211

ABSTRACT

A new approach for generating high-speed multispectral images has been previously reported by our team. The central concept is that spectra can be acquired for each pixel in a confocal spatial laser scan by using a fast spectrometer based on optical fiber delay lines. This method merges fast spectroscopy with standard spatial scanning to create image datacubes in real time. The datacubes can be analyzed to define regions of interest (ROIs) containing diseased tissue. Firmware and software have been developed for selectively scanning these ROIs with increased optical power. This enables real time image-guided laser treatment with a spatial resolution of a few microns.

Keywords: Multispectral scanning, fluorescence, tissue imaging, laser treatment

1. INTRODUCTION

Cancer at the tissue and cellular levels can be detected with fast multispectral confocal mapping.¹ Biomedical researchers hope to detect abnormal tissue architecture or composition, tumor angiogenesis, take optical biopsies, perform treatments, and monitor long-term results. Achieving tissue characterization without the use of extrinsic contrast agents is desirable, for both intrinsic and logistic reasons. For example, the fluorescence spectra of healthy tissue, metaplastic tissue, dysplastic tissue, and invasive carcinoma have been published.² These spectra indicate that ten wavelength bins distributed from 500 to 800 nm would reliably distinguish amongst the various tissues, and allow for high specificity and sensitivity. After large masses are removed with conventional surgical methods, cancerous margins could be identified and possibly treated with new optical tools. It is well known that tumor-margins can be highly convoluted due to factors in their microenvironment that control growth.³ Interspersing (“fingering”) of tumors into adjacent tissues is common and not immediately obvious to the surgeon at the macro-scale. High spatial resolution would be required for treating infiltrated tumor margins.⁴ Potential optical treatments include laser ablation^{5,6} and/or photodynamic therapy.⁷

The above goals simultaneously require sufficient spatial, spectral, and temporal resolution. Confocal microscopy can map millimeter sized fields-of-view with ~ micron spatial resolution. Spectroscopic tools can provide multispectral data during laser excitation of fluorescence. Further, these spatial and spectral measurements should allow for the detection of millisecond dynamics in living systems. Rapid data transfer is especially important between the detection and treatment steps that we propose in this paper. All of these characteristics are not yet available in one cost-effective instrument, mostly because the spectroscopic tools are not fast enough.

A new approach for generating high-speed multispectral images has been previously reported by our team.⁸ The central concept is that spectra can be acquired for each pixel in a confocal spatial scan by using a fast spectrometer based on optical fiber delay lines. The spectrometer uses a serial array of reflecting spectral elements, delay lines between these elements, and a single element detector. Since the spectrometer is fiber-based, the face of the entrance fiber can act as the pinhole in a confocal microscope, in either a table-top or endoscopic implementation. This approach merges fast spectroscopy with standard spatial scanning to create image datacubes in real time. The datacubes can be analyzed to define regions of interest (ROIs) containing diseased tissue. These segmentations are based on ratios of fluorescent intensity in various spectral bands, and also occur in real time. Firmware and software have been developed for selectively scanning these ROIs with increased optical power. One can imagine three sequential scans that would detect disease, treat disease, and assess the treatment. This achieves a tight coupling – both spatially and temporally – between detection and intervention, a desirable capability that has been a long-term goal of ours. The approach would enable real

* gcarver@omegafilters.com; phone 1 802 251-7346; www.omegafilters.com

time treatment with a spatial resolution of a few microns. An initial demonstration of feasibility is presented using known test specimens.

The following sections describe the design, attributes, performance and advantages of this new instrument – emphasizing new firmware enabling treatment with high spatial resolution. Examples are given showing localized bleaching of fluorescent beads, and laser ablation of fixed tissue. This effort was partially funded by the National Cancer Institute through the National Institutes of Health (SBIR Phase II grant number 5R44CA124036-03).

2. OPTICAL DESIGN

A schematic of our multispectral confocal scanner is shown in figure 1. The following sub-sections briefly review the confocal, endoscopic, and spectroscopic sub-systems. This review is followed by a conceptual description of our new treatment mode, which is enabled by upgraded firmware.

As with fluorescence microscopes, our excitation beam enters the system by reflecting from a dichroic splitter. The excitation is provided by a pulsed 488 nm or 405 nm laser. Averaged over 1 second, excitation levels at the tissue are in the 1 to 2 milliwatt range. Optical power should be limited to about 5 milliwatts for operating room safety reasons and to avoid potential tissue damage⁹ in the subject.

The basic concept of confocal scanning is shown by the two scanning mirrors and associated optics in figure 1. As the two mirrors are scanned in an x-y raster pattern, the focused spot on the sample is always conjugate with a pinhole or small area detector (the pinhole in figure 1 is the fiber aperture marked with an asterisk). The pinhole limits the acceptance of light from axial and lateral locations away from the position of the focused spot. Since fluorescence from biological materials typically occurs within 1 to 5 nsec after excitation, both reflected and photoexcited signals propagate back to the pinhole before the mirrors can move appreciably. This allows the mirrors to de-scan back-propagating photons such that light from the focused spot indeed stays conjugate with the pinhole. As a result, scanning confocal systems can generate maps (or “images”) with spatial resolution at or near the laser spot size. In this system, the 488 nm laser is focused at NA = 0.24 to a 1.2 micron diameter spot and scanned over an adjustable field (that can be zoomed from 50 to 500 microns). Since the scanning process actually generates a spatial convolution of the focused spot with features in the sample, it is possible to detect features below the diffraction limit (though they appear equal in size to the spot). These ideas¹⁰ have been applied to images of functional nuclear architecture¹¹, and have been used for years in the materials and semiconductor industries.¹²

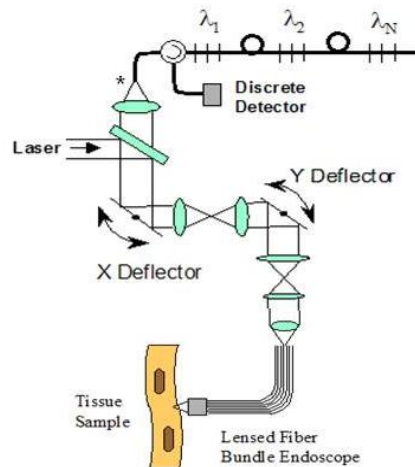


Figure 1. Multispectral confocal scanning system

The system depicted in figure 1 performs microscopy when a sample is placed at the focus of the objective lens, and endoscopy when the proximal end of an endoscope is placed in the same location. For endoscopy, a coherent fiber bundle with 30,000 three micron diameter fibers is placed under the lens. The confocal scanner raster scans the proximal end of the endoscope. A given fiber within the bundle transfers the laser to the distal end where a lensed tip relays the beam from the fiber to the tissue. Fluorescence or reflected light from a resolution element is imaged back into the same fiber, propagates back to the proximal end, is collected and de-scanned by the confocal optical system, and is finally focused on the confocal pinhole. This entire process occurs within the dwell time of the raster scan (2.5 microseconds in our design). During endoscopy, the 488 nm laser is focused by the distal tip at NA = 0.8 to a 0.4 micron diameter spot and scanned over an adjustable field (that can be zoomed from 10.8 to 108 microns) at a working distance of 80 microns. The transmission of this endoscope is consistent with reports in the literature.¹³ The following sub-section describes our new spectrometer, which conveniently maps proximal reflection and emission bands into different temporal bins.

Our fiber optic spectrometer is based on a serial array of reflecting spectral elements, delay lines between these elements, and a single element detector.⁸ After excitation by a laser pulse, broadband fluorescence from a biological tissue sample propagates into the array via the confocal aperture, light of the first wavelength band reflects from the first element, and light of the Nth wavelength band reflects from the Nth element. Each wavelength is mapped into a specific time slot. Each delay line is equal to the length of the laser pulse. The spectral elements can be fabricated in two ways - fiber tips can be coated with interference filters to create > 10 nm wide spectral slices, while fiber Bragg gratings can be written into the fiber core to create 1 to 2 nm wide spectral slices.¹⁴

The key advantage of this design is speed – a spectrum is acquired during the dwell time of each pixel in the spatial scan. Beyond speed, this new design has several other advantages. First, wavelength bin centers and widths can be arranged in an arbitrary manner with varying widths matched to a given application. Second, the wavelength separation method has no influence on spatial scanning fidelity. A map of a given color will spatially register with a map of another color. Third, each polarization state is reflected in a similar manner. Fourth, the new design is compatible with confocal optics. Further, the system can also be used to treat diseased tissue with high spatial resolution – as we demonstrate below.

The optical system described above is controlled by software running on a 1.73 GHz quad-core Intel i7-820 processor, and firmware running on a custom electronics box. The software, written in LabView, generates a graphical user interface (GUI). The firmware runs on board-mounted FPGA and DSP chips within the electronics box, which also provides several interconnects to the optical package and the quad box. These interconnects include inputs (start trigger, USB, fiber to PMT), and outputs (scan mirror control signals, laser trigger, PMT analog output, A-to-D start trigger, sampling clock). A 14-bit digitizer card capable of 100 MS/s is mounted within the quad box chassis. Several events occur during operation: the GUI issues a start pulse, the electronics box sends control signals to the laser and mirrors, and the digitizer card receives synchronizing pulses that stimulate acquisitions of the PMT output. The quad box receives a serial array of acquisitions from the digitizer, and casts the data into a three-dimensional datacube. Selected slices of the data cube and a bin histogram are displayed on the GUI in real time. The GUI includes settings for allocations amongst space, wavelength, and over sampling – which are forwarded via the USB to the electronics box. Default settings are: 200 pixels per line, 150 lines per datacube, 10 spectral bins per pixel, and 10 samples per bin. The GUI allows multiple image display modes: any selected spectral bin in grey levels, the sum of all selected spectral bins in grey levels, three selected spectral bins assigned to RGB levels, and any combinations of bins can be entered into formulae to generate RGB levels for pseudo color display. Spectral angle mapping (SAM)¹⁵ is a proven way to emphasize subtle spectral differences within images, and is included in our suite of real time tools. Naturally, other spectral discrimination/analysis methods can also be applied to the collected data.

Figure 2 is a conceptual depiction of our new treatment mode, which includes three scans. The first scan generates a multispectral fluorescent image that is enhanced via SAM analysis to clearly show where diseased tissue exists (red areas in the figure). Software sends the addresses of these locations to the electronics control box over a high speed USB connection. A second scan covers the same area while firing the laser (with increased power and longer dwell time) at only the specified locations. The third scan confirms that the diseased areas are ablated/altered (grey areas) and detects residual disease that may require a follow-up treatment. Each of the three scans would occur at 10 frames per second such that the subject does not move between the sensing and treatment scans. The figure attempts to show an infiltrating surgical margin within a roughly 200 micron field of view. Surgeons would have the ability to approve or disapprove treatment for each field, or region-of-interest within a field, while the endoscopic procedure is ongoing.

In general, lateral spot size is proportional to $f/\#$ while longitudinal spot size is proportional to the $f/\#$ squared.¹⁶ As mentioned above, our lateral spot size is 1.2 microns (microscopy mode) and 0.4 microns (endoscopy mode). Discounting scatter for epithelial applications, the longitudinal depth of focus would be expected to be about 4 microns (microscopy mode) and 0.4 microns (endoscopy mode).

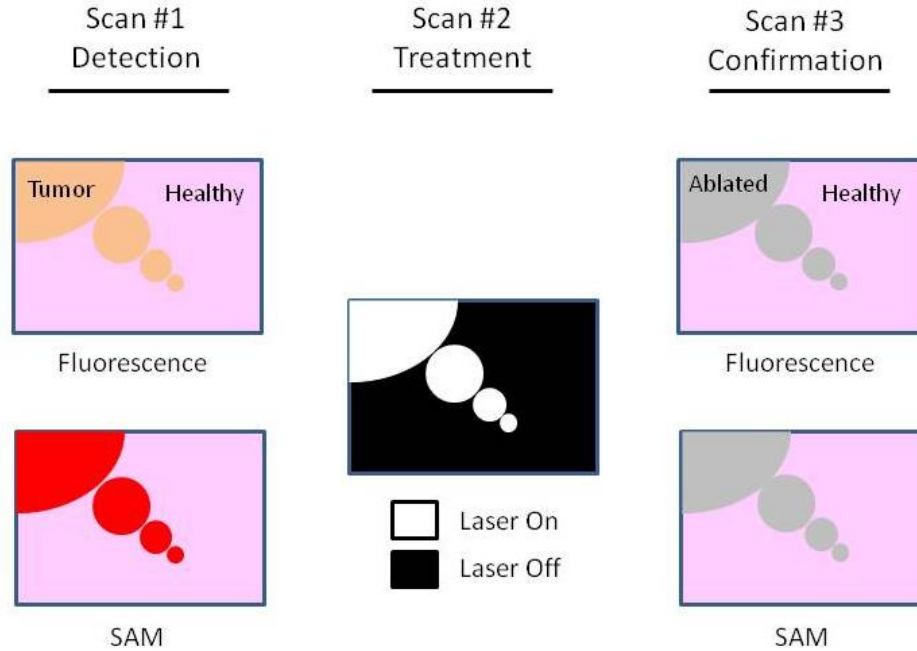


Figure 2. Treatment Concept

3. RESULTS

At a typical sampling rate of 60 MHz, each image generation mode functions at 10 frames per second. This temporal rate is sufficient for avoiding image artifacts caused by a subject's pulse and respiration while diagnosing disease and/or directing treatment.

We previously confirmed that our system resolves 1 micron bars on a known test target. Figure 3 shows fluorescent beads imaged in microscopy mode. The beads were drop-cast from solution onto a glass slide, are 3 microns in diameter, and emit fluorescence that is captured by one of our spectral bins (rendered in green for the figure). The arrows in figure 3 indicate two beads – selected due to their being adjacent to other beads – that were observed before exercising the treatment mode (left side of the figure), but not observed after exercising the treatment mode (right side of the figure). The treatment scan was performed while increasing both the average laser intensity (from 8 to 60 mW), and pulse length (from 160 nano-seconds to 2.5 micro-seconds). Typical dosage is 13 J/cm^2 during the pixel dwell time. We see that the system is capable of bleaching a bead positioned within a couple of microns from an adjacent bead – while causing only moderate dimming to the adjacent bead. This confirms the lateral resolution of the treatment mode (in both lateral directions, due to the positioning of the referenced beads).

We also acquired images on unstained, fixed and sectioned rat mammary tissue using six spectral bins. Figure 4 renders these images where the three strongest bins are applied to the RGB pixels in our pseudo color display. The before/after treatment images at the top of the figure show an example where a relatively small area was ablated. The images at the bottom of the figure show a larger area encompassing the duct walls. These images further confirm lateral resolution,

but say nothing about depth (axial) resolution since these are thin sections. Experiments are planned for assessing axial resolution, which should be near our depth-of-focus if the dosage is set just above the ablation threshold.



Figure 3. Microscopy of fluorescent beads before (left) and after (right) selective laser ablation of two beads marked with arrows (scale bar is 100 μm)

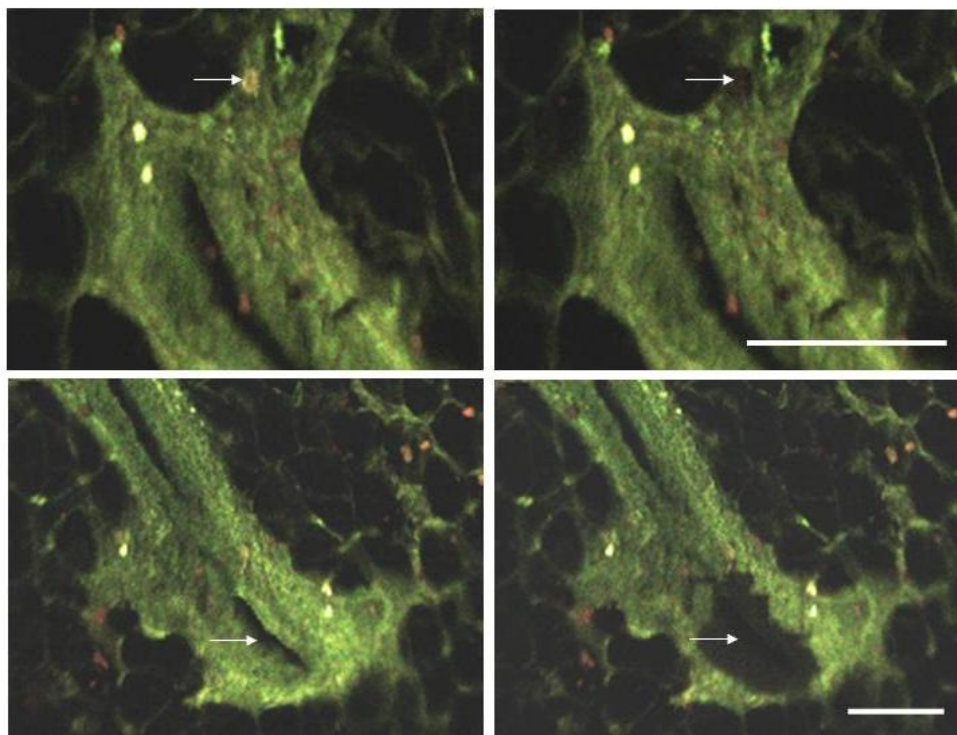


Figure 4. Microscopy of fixed and sectioned rat mammary tissue before (left) and after (right) selective laser ablation of two locations marked with arrows (scale bars are 100 μm)

4. CONCLUSIONS

The multispectral imaging system described in this paper has been previously designed, built, and tested for the spectral mapping of intrinsic tissue fluorescence (autofluorescence). The spatial resolution is sufficient for cellular level imaging. The spectral resolution is suitable for detecting the spectral signatures of cancer. The temporal resolution is

sufficient for avoiding any influence of the cardiovascular and respiratory rhythms of living subjects. In this paper, the system has been enhanced to enable a treatment mode. Treatment is performed via three steps: multispectral imaging to identify and locate diseased tissue, scanning with increased power and dwell time to ablate tissue in highly spatially resolved regions, and then multispectral imaging to confirm the treatment. This new treatment mode was demonstrated on fluorescent beads and fixed tissue with a lateral spatial resolution of 1 to 2 microns. Longitudinal sections will be assessed going forward.

This paper has presented the concept, optoelectronic instrumentation, and firmware for performing highly resolved sensing and treatment. Future work would actually apply treatment to in-vivo tissue – either with laser ablation and/or photodynamic therapy. Our ultimate goal is early detection of disease via optical biopsy, and immediate intrasurgical treatment of localized diseased tissue. Surgeons would continue excising identifiable tumors, while our approach could be applied in a step and repeat mode to treat infiltrative margins.

ACKNOWLEDGEMENTS

We thank Dr. Bob Johnson of Omega Optical for supporting this effort, and the National Institutes of Health for partial support under NCI 5R44CA124036-03.

REFERENCES

- [1] Chung, A., Wachsmann-Hogiu, S., Zhao, T., Xiong, Y., Joseph, A., Farkas, D.L., “Advanced optical imaging requiring no contrast agents - A new armamentarium for medicine and surgery,” *Current Surgery* 62, 365-370 (2005).
- [2] Zellweger, M., Goujon, D., Conde, R., Forrer, M., van den Bergh, H., Wagnieres, G., “Absolute autofluorescence spectra of human healthy, metaplastic, and early cancerous bronchial tissue *in vivo*,” *Applied Optics* 40 (22), 3784-3791 (2001).
- [3] Anderson, A.R.A., Weaver, A.M., Cummings, P.T., Quaranta, V., “Tumor morphology and phenotypic evolution driven by selective pressure from the microenvironment,” *Cell* 127, 905–915 (2006).
- [4] Jacobs, L.K., Carney, P.S., Cittadine, A.J., McCormick, D.T., Somera, A.L., Darga, D.A., Putney, J.L., Adie, S.G., Ray, P., Craddock, K.A., Tafra, L., Gabrielson, E.W., Boppart, S.A., “Intraoperative assessment of tumor margins with a new optical imaging technology: A multicenter, randomized, blinded clinical trial,” *Cancer Research* 72 (24), (2012).
- [5] Norberto, L., Polese, L., Angriman, I., Erroi, F., Cecchetto, A., D’Amico, D.F., “Laser photoablation of colorectal adenomas: A 12-year experience,” *Surgical Endoscopy and Other Interventional Techniques* 19 (8) 1045-1048 (2005).
- [6] Zhuo, S., Chen, J., Wu, G., Zhu, X., Jiang, X., Xie, S., “Label-free multiphoton imaging and photoablation of preinvasive cancer cells,” *Applied Physics Letters* 100, 023703 (2012).
- [7] Liu, B., Farrell, T.J., Patterson, M.S., “Comparison of photodynamic therapy with different excitation wavelengths using a dynamic model of aminolevulinic acid-photodynamic therapy of human skin,” *Journal of Biomedical Optics* 17 (8), 088001 (August 2012).
- [8] Carver, G.E., Locknar, S.A., Morrison, W.A., Farkas, D.L., “High-Speed Multispectral Confocal Imaging,” *Proc. SPIE 8587, Imaging, Manipulation, and Analysis of Biomolecules, Cells, and Tissues XI*, 858715 (2013).
- [9] Vogel, A., Venugopalan, V., “Mechanisms of pulsed laser ablation of biological tissues,” *Chem. Rev.* 103, 577-644 (2003).
- [10] Pawley, J.B., [Handbook of Biological Confocal Microscopy, 2nd Ed.], Plenum Press, New York, (1995).
- [11] Cremer, T., Kreth, G., Koester, H., Fink, R.H.A., Heintzmann, R., Solovci, I., Zink, D., “Chromosome territories, interchromatin domain compartment and nuclear matrix: An integrated view of the functional nuclear architecture,” *Critical Review in Eukaryotic Gene Expression* 12 (2), 179-212 (2000).
- [12] Carver, G.E., “Scanned photoluminescence with high spatial resolution in semi-insulating GaAs and InP: aspects of surface passivation and photodegradation,” *Semicond. Sci. Technol.* 7, A53-A58 (1992).
- [13] Udovich, J.A., Kirkpatrick, N.D., Kano, A., Tanbakuchi, A., Utzinger, U., Gmitro, A.F., “Spectral background and transmission characteristics of fiber optic imaging bundles,” *Applied Optics* 47(25), 4560-4568 (2008).

- [14] Carver, G.E., Farkas, D.L., Porque, J., Feder, K.S., Westbrook, P.S., "Visible wavelength fiber Bragg grating arrays for high speed biomedical spectral sensing," in Bragg Gratings, Photosensitivity and Poling in Glass Waveguides, OSA Technical Digest, paper BThB5 (2010).
- [15] Weyermann, J., Schlapfer, D., Hueni, A., Kneubuhler, M., Schaepman, M., "Spectral angle mapper (SAM) for anisotropy class indexing in imaging spectrometry data," Proc. SPIE 7457, Imaging Spectrometry XIV, 74570B (2009).
- [16] Smith, W.J., [Modern Optical Engineering, 3rd Ed.], McGraw-Hill, New York, 161 and 348, (2000).